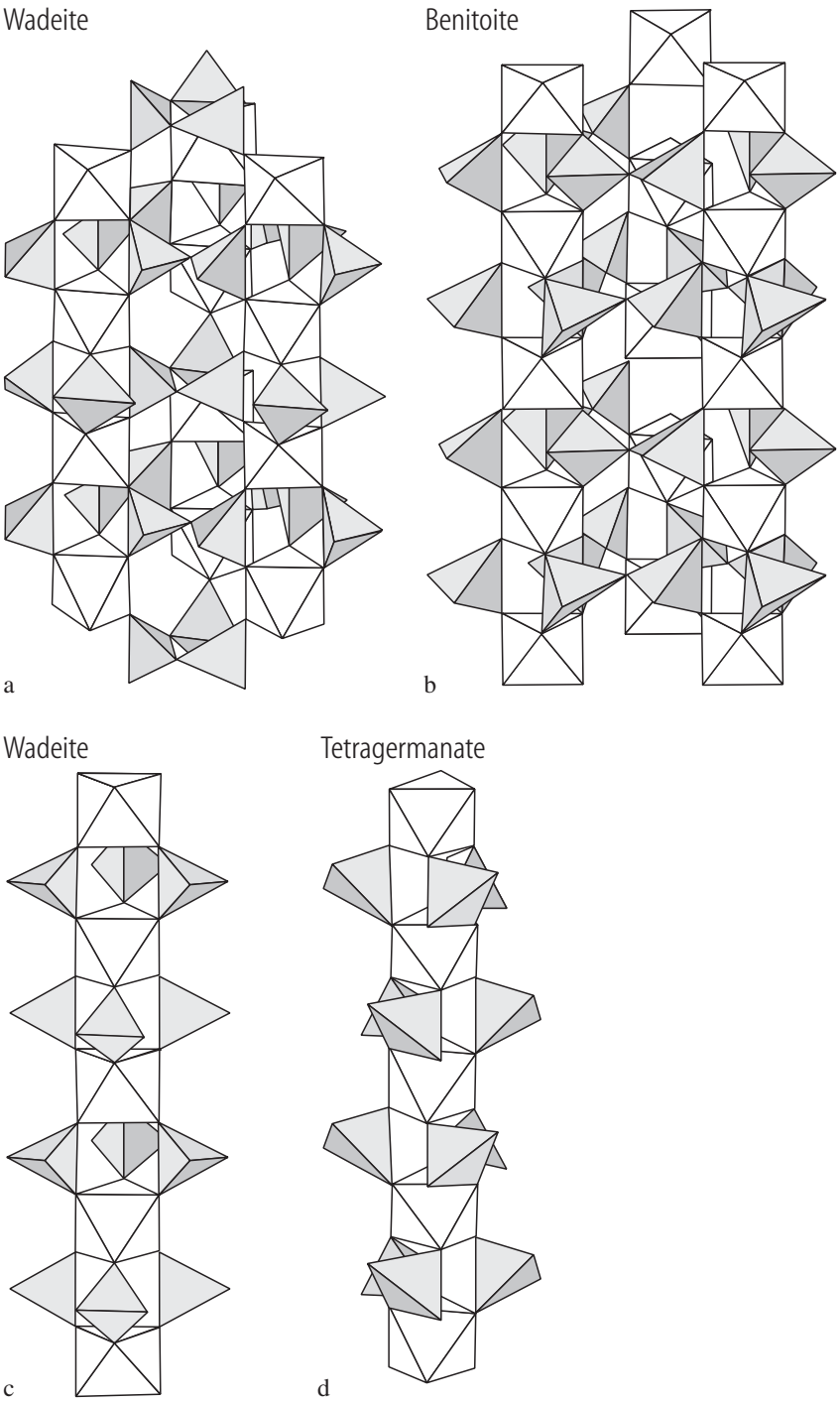

Fig. 1. Wadeite **(a)**, benitoite **(b)**. Fragments of the frameworks embracing two closed spaces in the first and one infinite channel in the second. Two kinds of infinite columns of M octahedra and triads of Si tetrahedra binding them together are shown for wadeite, straight **(c)** and tetragermanate, twisted **(d)** [77B1].

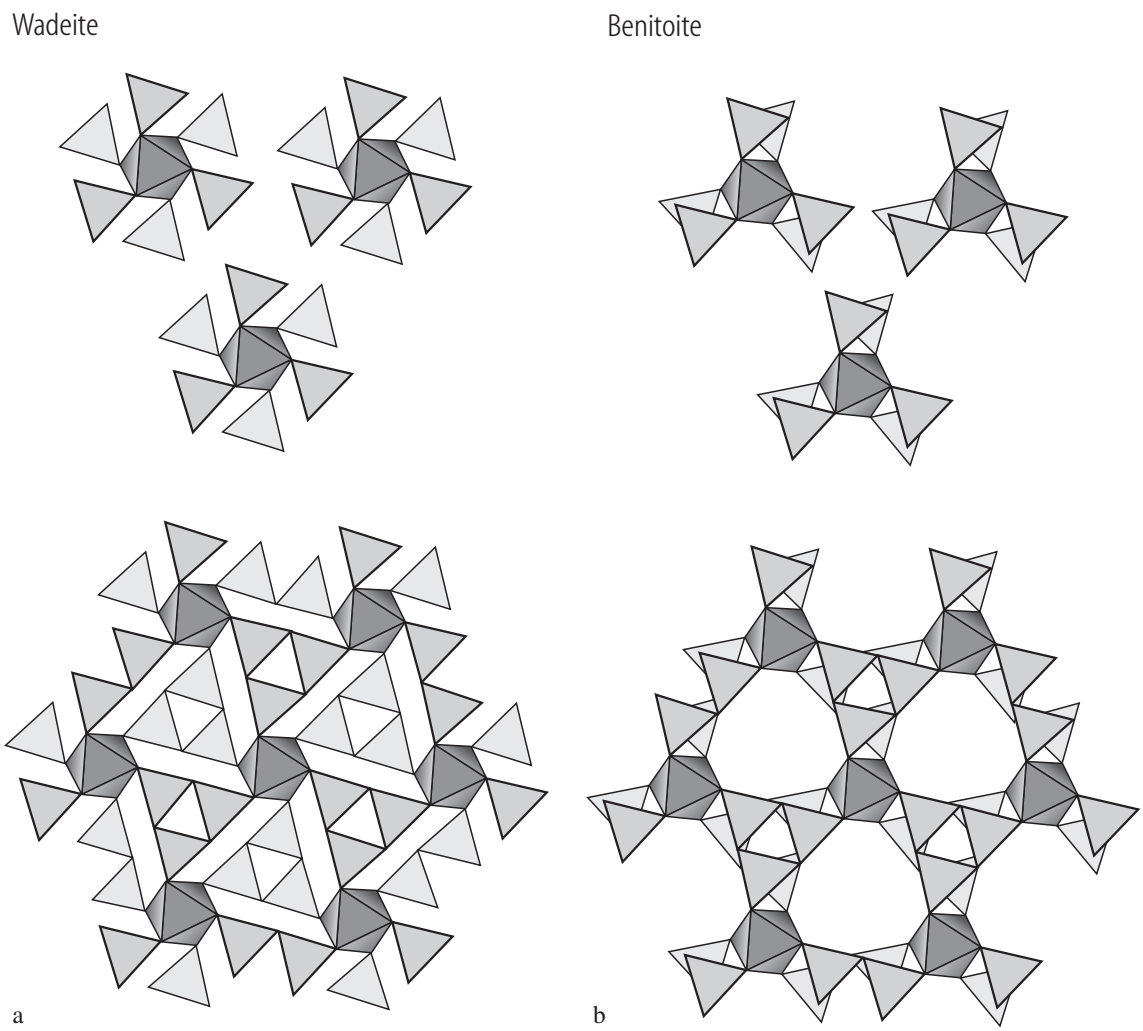

Fig. 2. Wadeite **(a)**, benitoite **(b)** mixed framework as result of the condensation of infinite columns with different directions of rotation of the tetrahedra around the vertical edge [77B1].

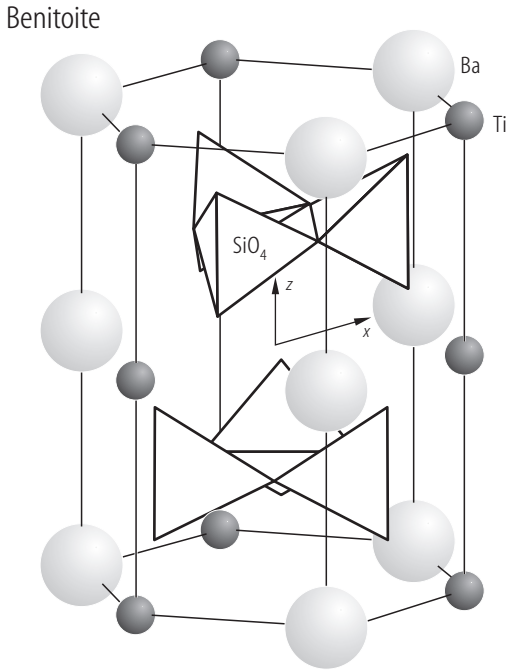

Fig. 3. Benitoite, $BaTiSi_3O_9$. Schematic diagram of the structure. The rings are shown as three linked tetrahedra. The ***c***-axis is the threefold symmetry axis and is set to be the ***z***-axis. The twofold symmetry axis is along the line connecting Ba to Ti in the (***ab***) plane and is set to be the ***x***-axis [69F1, 93K1].

For Fig. 4 see next page

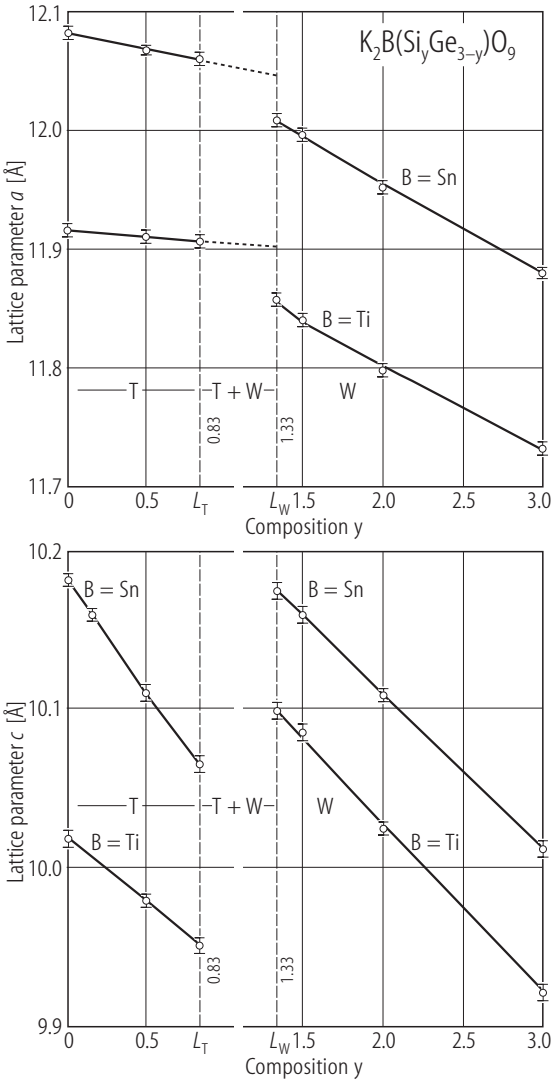

Fig. 5. $K_2B(Si_yGe_{3-y})O_9$ with B = Ti(1) and B = Sn(2). Lattice parameters as function of silicon content. W: wadeite-type structure; T: tetragermanate structure [75C1].

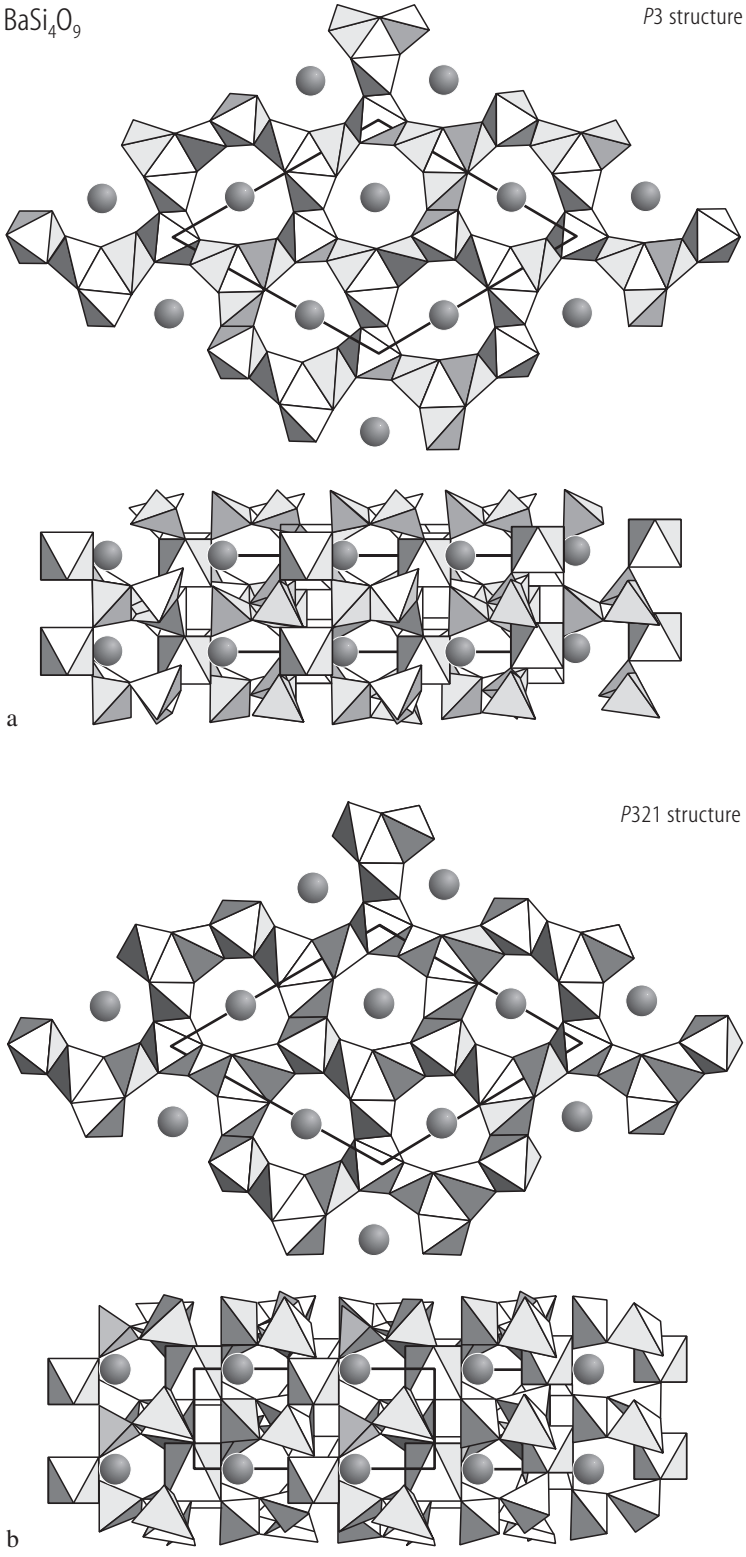

Fig. 4 a, b. For caption see next page

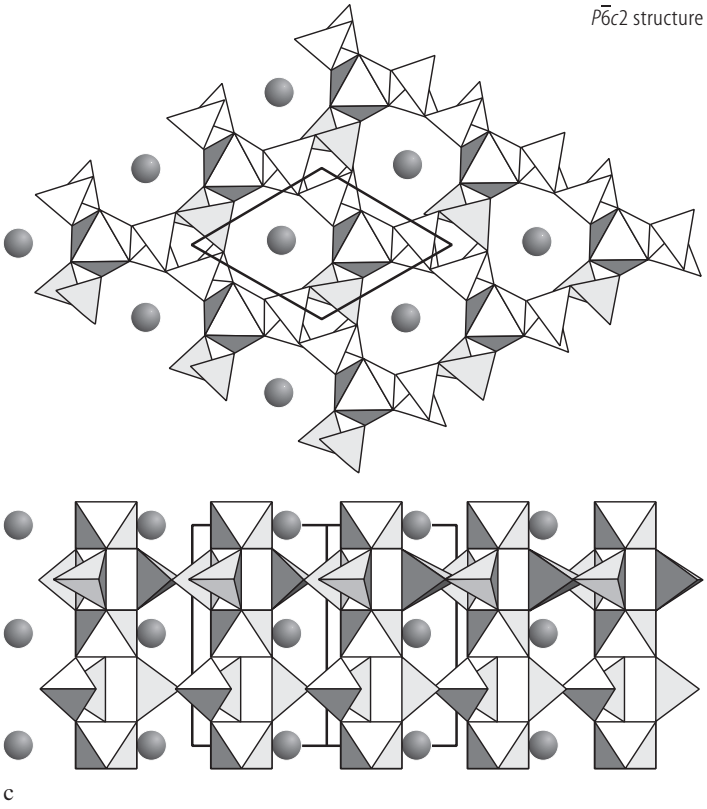

←
Fig. 4. $BaSi_4O_9$. Comparison of the crystal structures in the trigonal P3 structure **(a)**, in the benitoite structure hexagonal $P\bar{6}c2$ **(c)** and the $SrGe_4O_9$, trigonal P321 structure **(b)** [99H1].

Fig. 6. Walstromite. Idealized representation of the structure projected onto $(10\bar{1})$ showing how the layers of three-membered rings fit together. The direction of ***y*** is indicated [68D1].
↓

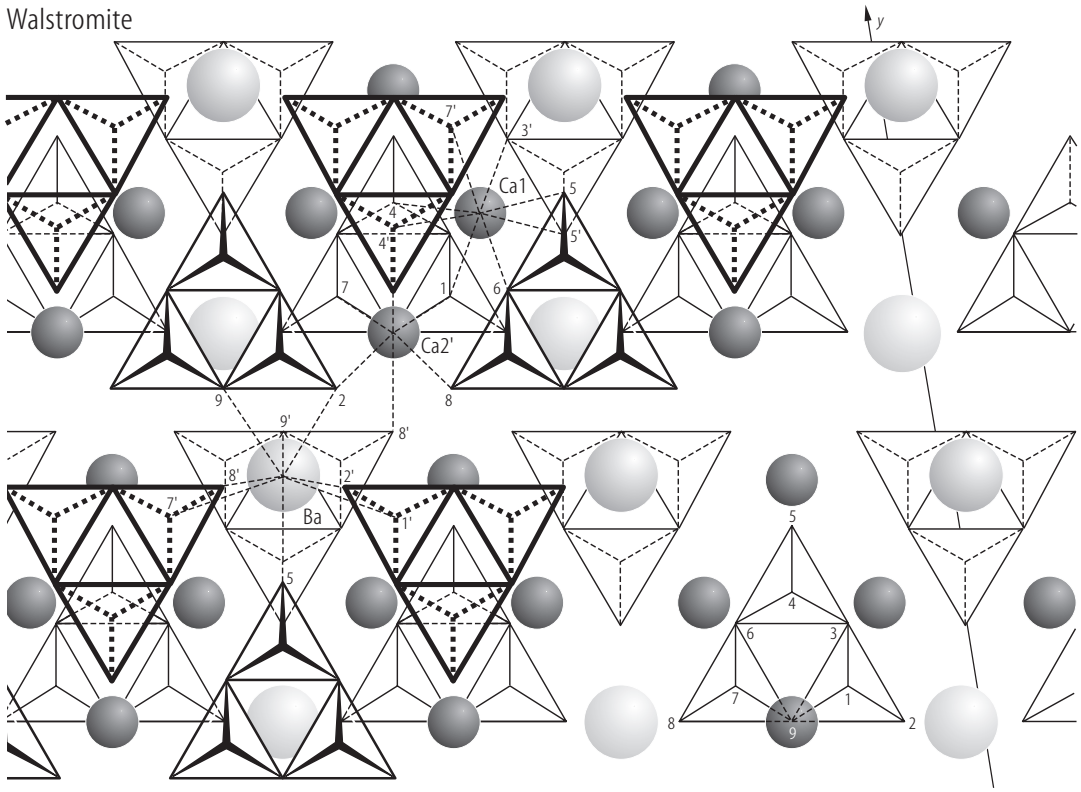

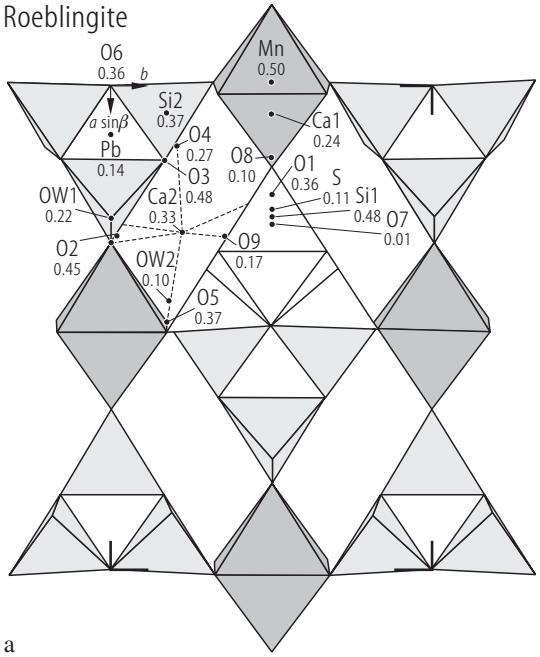

a

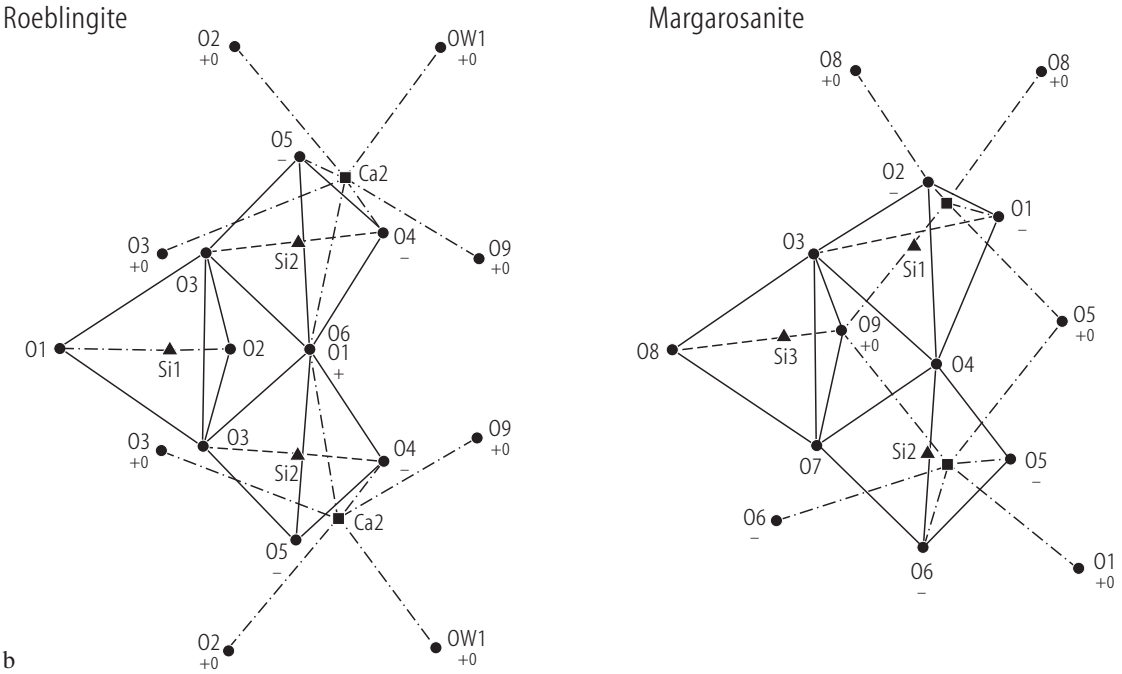

b

Fig. 7. Roeblingite. **(a)** Polyhedral diagram with labelled asymmetric unit projected down [100]. The MnO_6 octahedra are dark shaded and the $[Si_3O_9]$ 3-rings are light shaded. Note that some $[Si_3O_9]$, related by inversion at (000) have been omitted and one $[Si_3O_9]$ at (1/2 1/2 0) is not shaded. This attempts to emphasize the $^2_\infty[Mn(Si_3O_9)_2]$ fbb, the reason of micaceous cleavage on {001}. **(b)** Similar clusters in roeblingite (left) projected down [100] and margarosanite (right) projected down [100]. The $Si1Si2_2O_9$ rings and Ca2, Ca2 large cations in roeblingite, and $Si1Si2Si3O_9$ rings and Ca2, Ca1 large cations in margarosanite (squares) are partly isomorphic. Ca-O bonds are shown as dot-dash lines and relative heights of oxygens to bonded calcium were noted [84M2].

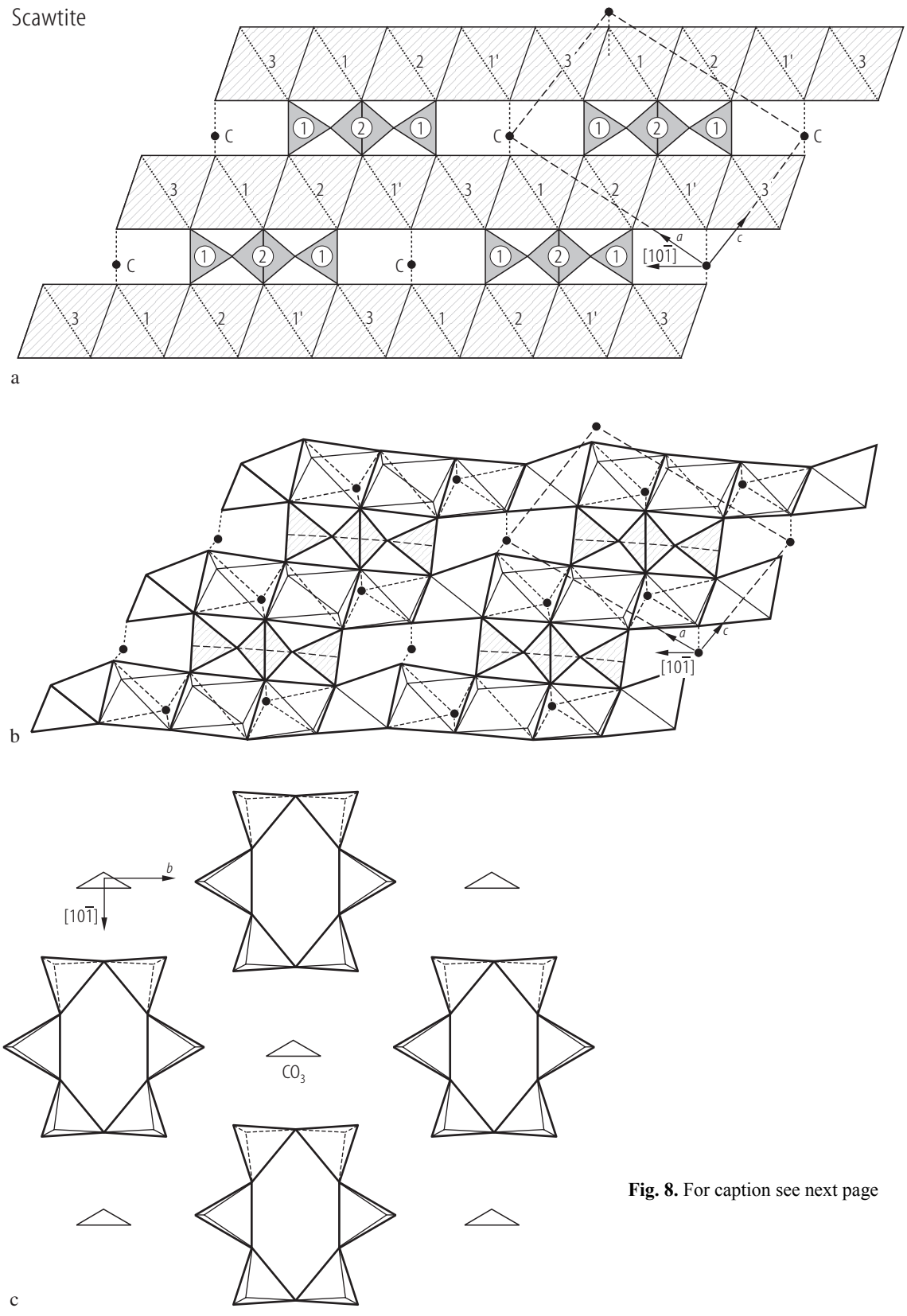

Fig. 8. For caption see next page

Fig. 8. Scawtite. Idealized **(a)** and actual **(b)** projection down the ***b***-axis. In the idealized projection layers of polyhedra may be seen lying in (101). The hatched layer represents calcium-oxygen polyhedra severely idealized to regular octahedra sharing edges. Six silicate tetrahedra (shared) are linked to form Si_6O_{18} rings, which overlap in projection to show only three. The dotted line shows an end-on view of the CO_3 triangles and the solid squares in **(b)** represent water molecules. One unit cell is outlined by the dashed lines. In the actual projection it may be seen that the calcium-oxygen polyhedra are very distorted. Note that for the type-2 octahedron, two vertices point in the same direction, whereas for type 1, the two vertices point in opposite directions. In **(c)** the projections normal (101) showing the positions of Si_6O_{18} rings and CO_3 triangles [73P1].

Eudialyte

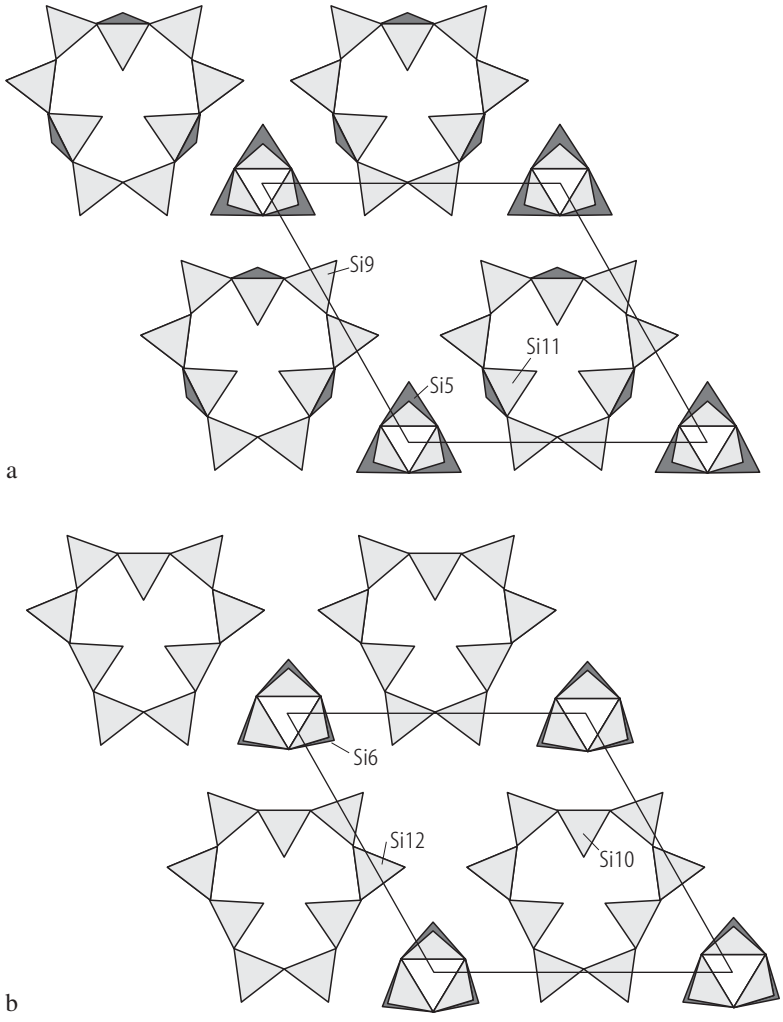

Fig. 9. For caption see next page

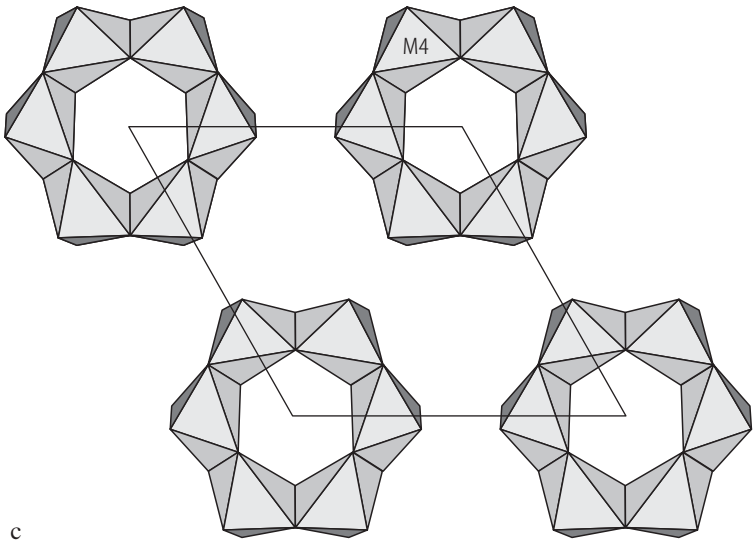

c

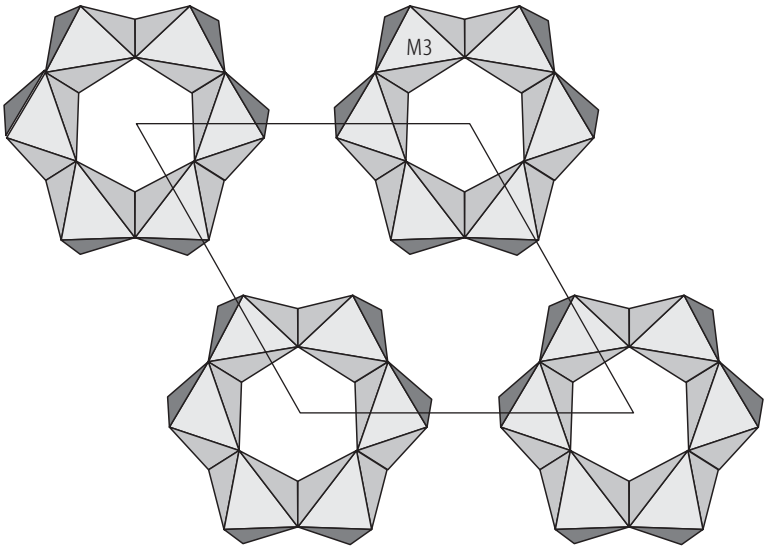

d

Fig. 9. Eudialyte. Sections of the Ti-rich eudialyte structure showing three-membered [Si_3O_9] rings and nine-membered [Si_9O_{27}] rings at $z \cong 0.05$ **(a)** and 0.55 **(b)**. Six-membered [M_6O_{24}] rings at $z \cong 0$ **(c)** and 0.5 **(d)** are also shown [99R2].

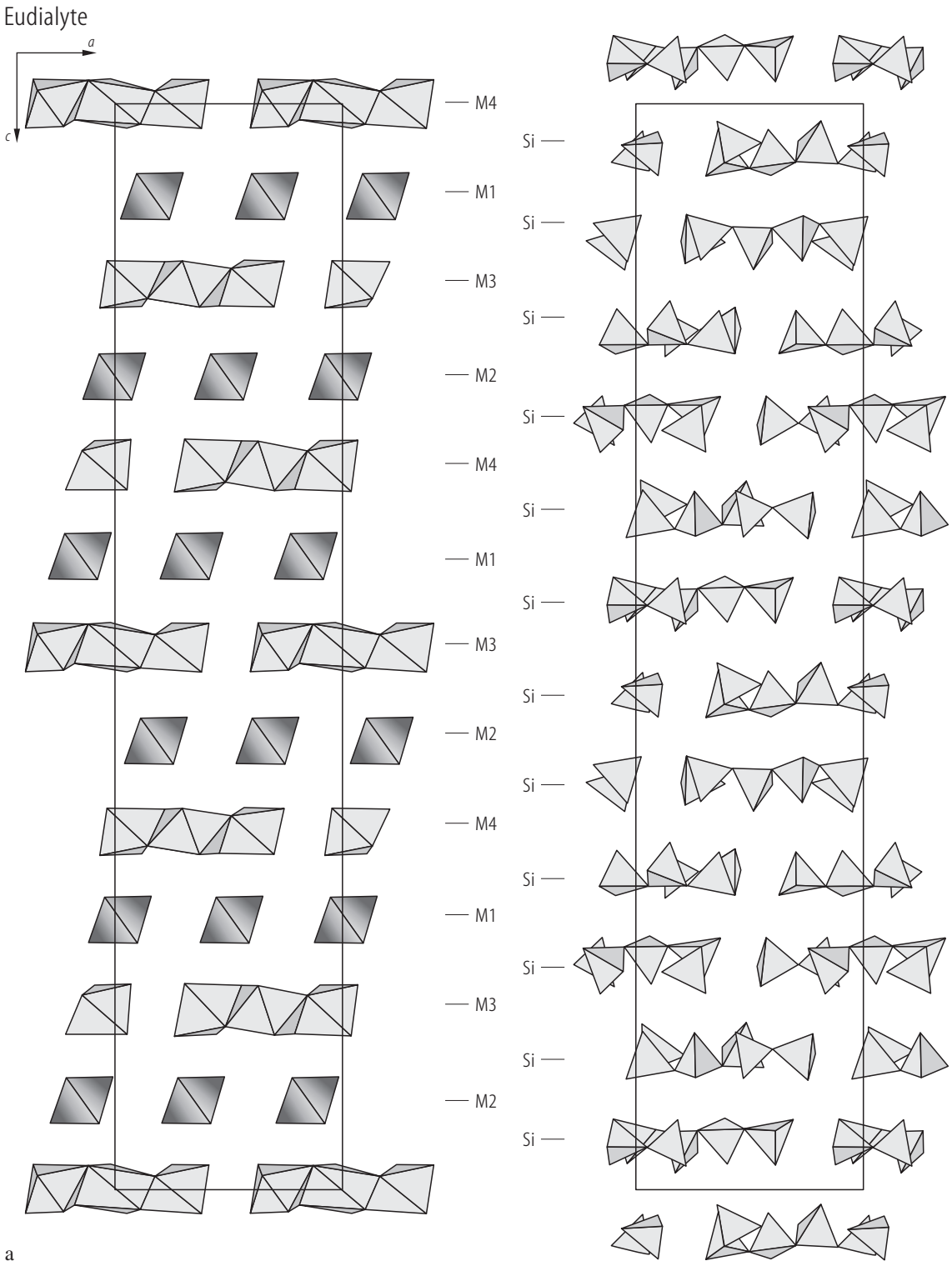

Fig. 10a. For caption see next page

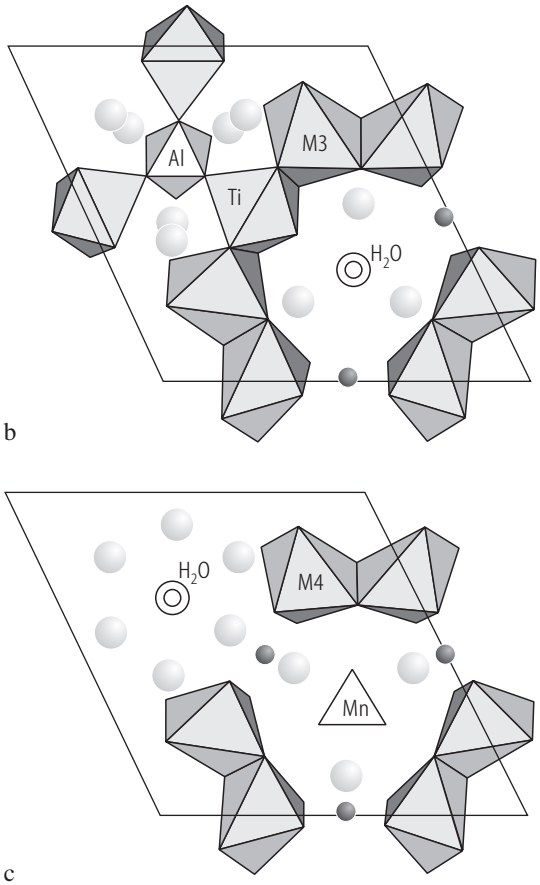

Fig. 10. Eudialyte. **(a)** The arrangement of Si and M1-M4 polyhedra along the ***c***-axis. **(b, c)** show fragments of the Ti-rich eudialyte structure of two different sections along ***c***: Al, Ti cluster **(b)** and Mn octahedron **(c)**. Dark circles-Fe, light circles-Na, double circles-H_2O [99R2].

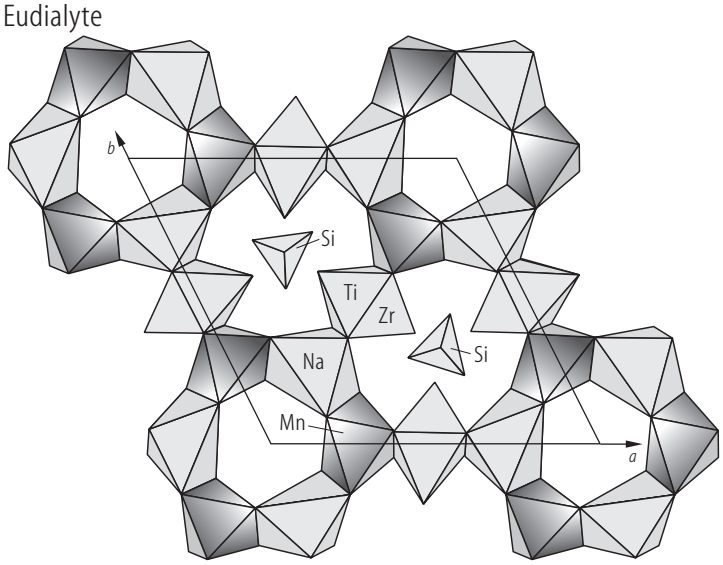

Fig. 11. Eudialyte. Mn, Na ordered analogue of eudialyte (symmetry R3). Fragment of the crystal structure projection onto the (001) plane. The octahedra occupied mainly by manganese atoms entering six-membered rings are dark shaded. The Si7,8-tetrahedra are located on threefold axes [00R1].

Catapleiite

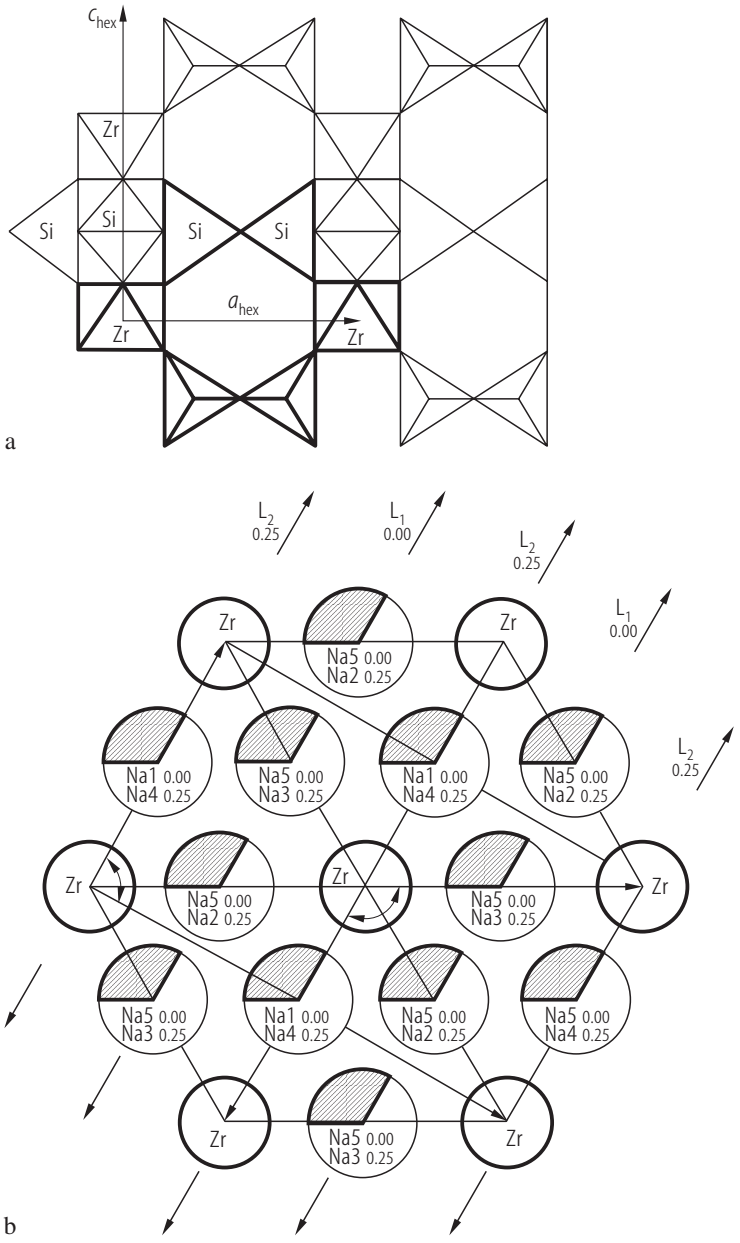

Fig. 12. Catapleiite. **(a)** Framework of M-octahedra of Zr and T-tetrahedra of Si. **(b)** Superposed projection of the two-dimensional Na sublattice along the ***b***-axis. Shown are axes of monoclinic and hexagonal cells [88I1].

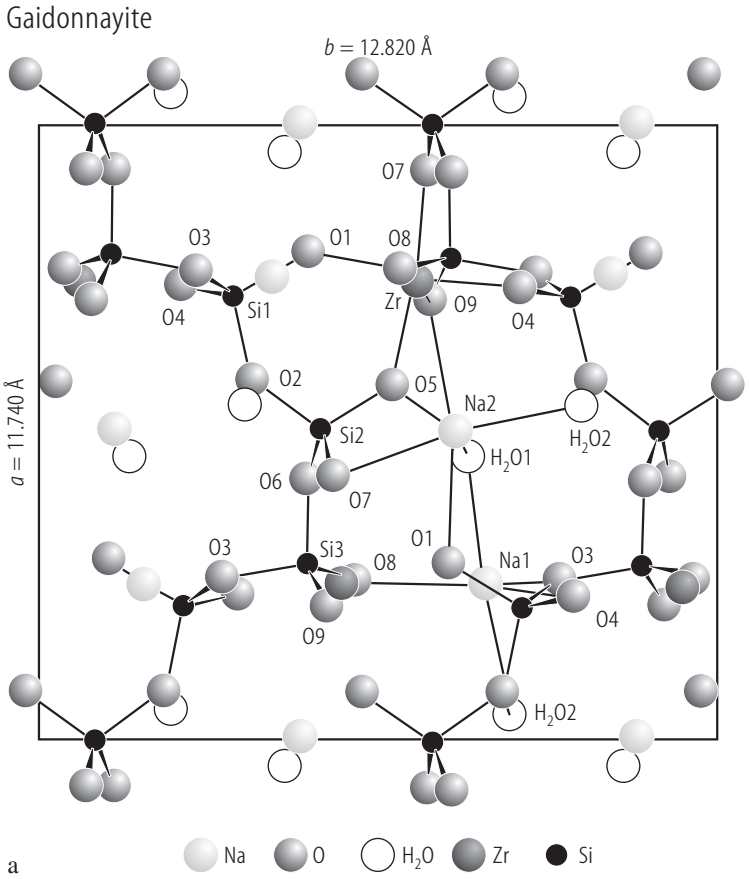

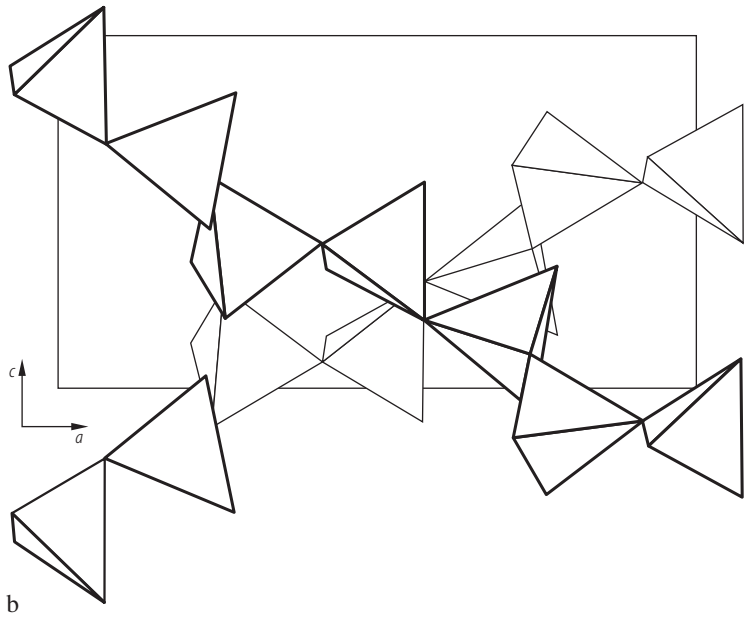

Fig. 13. Gaidonnayite. **(a)** Structure projected on (001). **(b)** The six-tetrahedron-repeat silicate chains projected onto (010) [85C1].

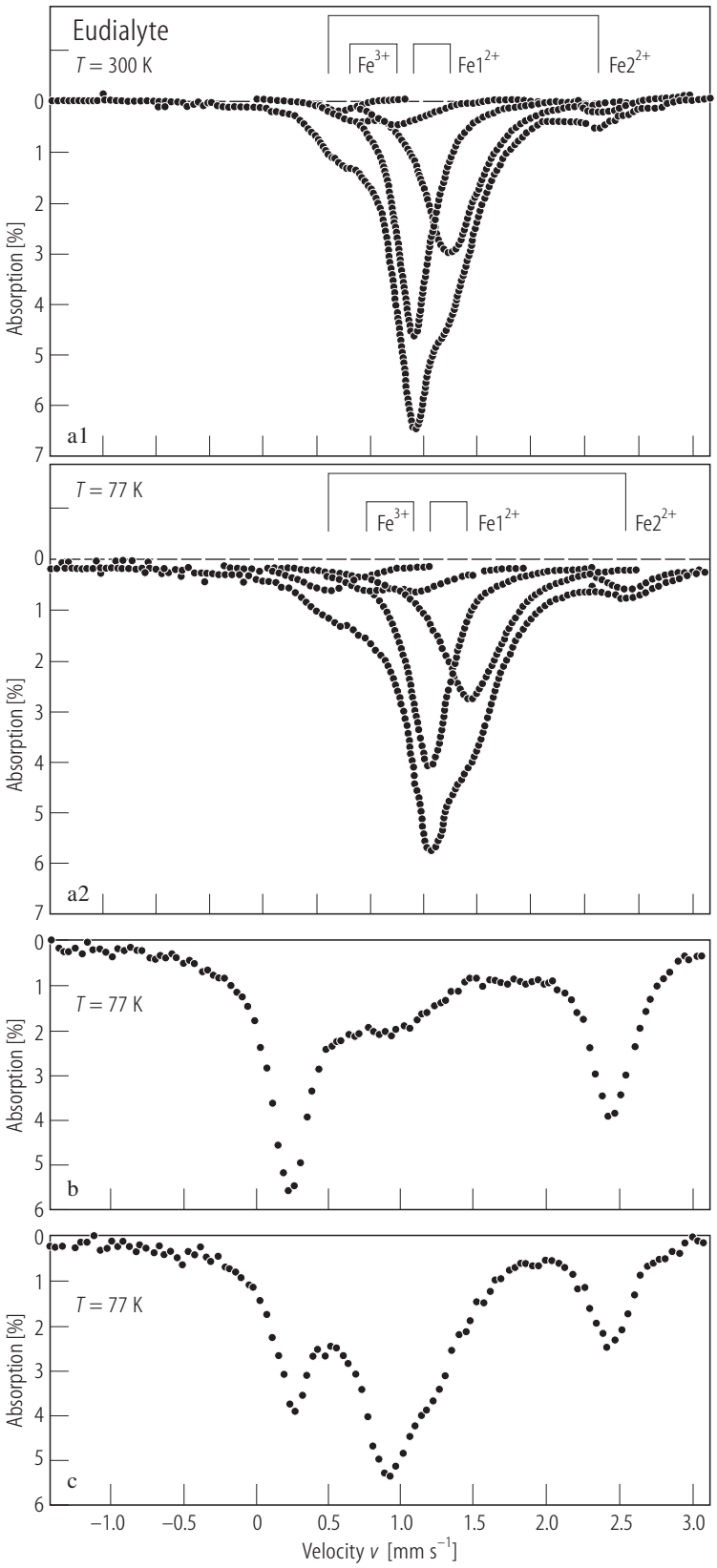

Fig. 14. Eudialyte. ^{57}Fe NGR spectra of **(a)** sample[12] (optically positive, group 1), **(b)** sample[14] (optically negative eucolite, group 2) and **(c)** sample[15] (red-brown optically negative intermediate variety; group 3) [91P1].

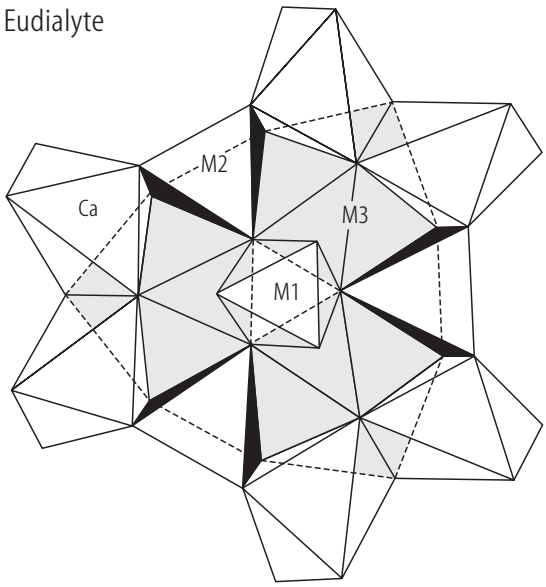

Fig. 15. Eudialyte. Clusters of M1 octahedra, M2 quadrangle pyramids and M3-eight-pointed polyhedra. M2 quadrangle pyramids are filled by $Fe2^{2+}$, Fe^{3+}, Mn^{2+} ions [91P1].

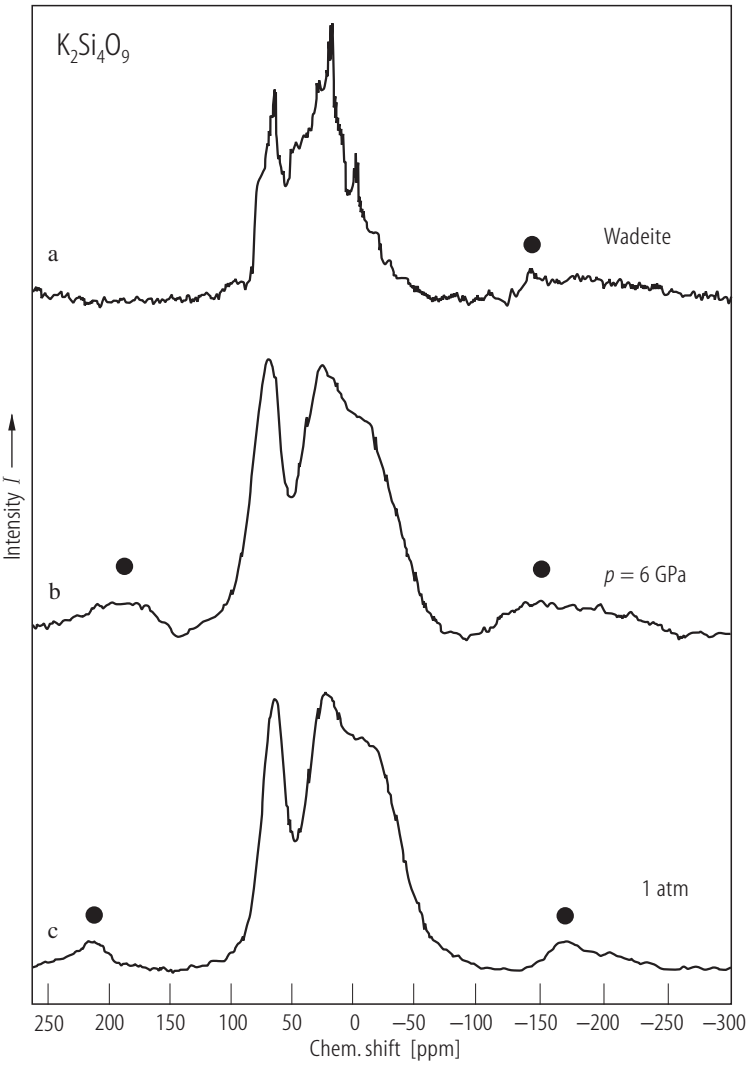

Fig. 16. $K_2Si_4O_9$. Crystalline **(a)** and glasses quenched from melts at 6 GPa **(b)** and 1 atm **(c)**. ^{17}O MAS NMR spectra. Spinning sidebands are marked by dots [94X1].

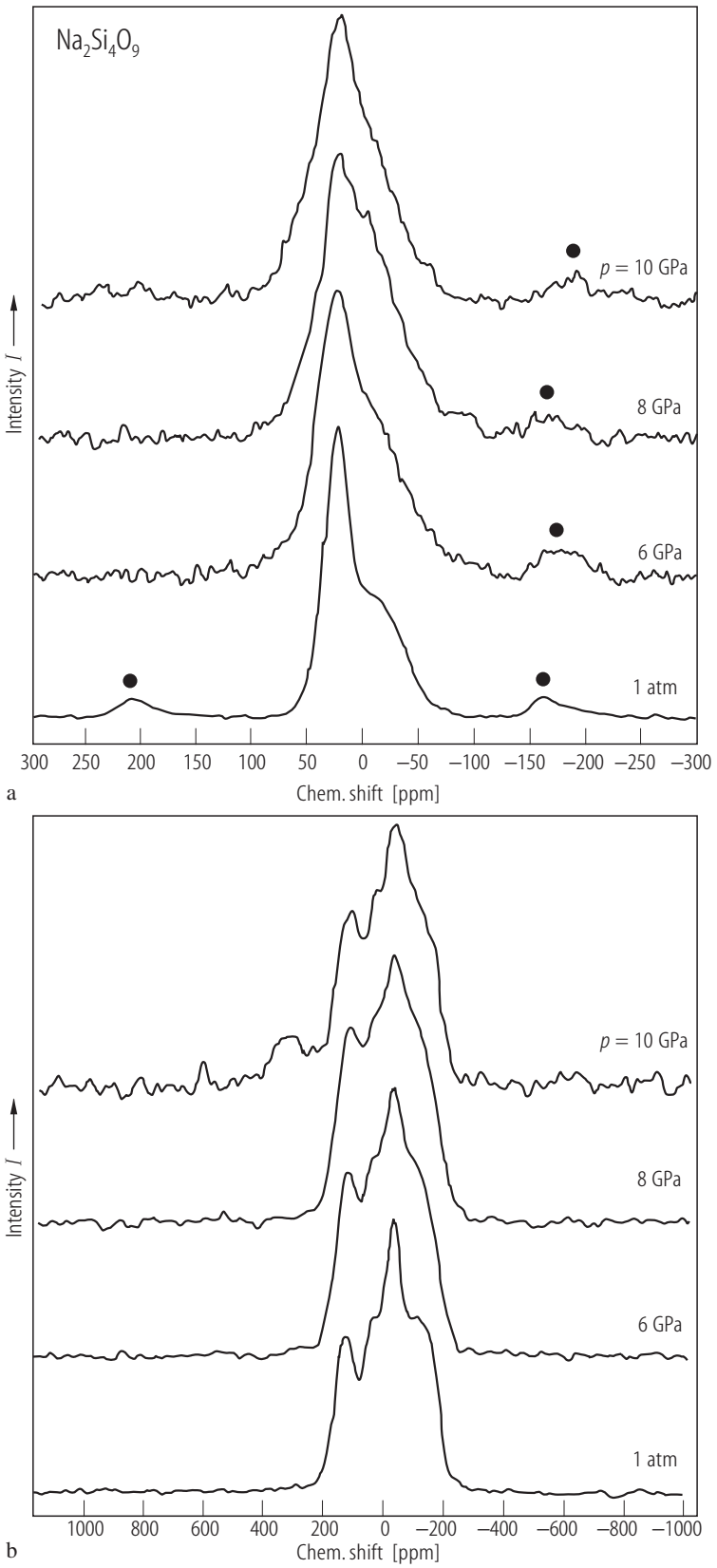

Fig. 17. $Na_2Si_4O_9$. Glasses. ^{17}O MAS NMR spectra **(a)** and ^{17}O NMR static spectra **(b)** of samples quenched from the melts at 1 atm, 6, 8 and 10 GPa [94X1]. Spinning sidebands are marked by dots.

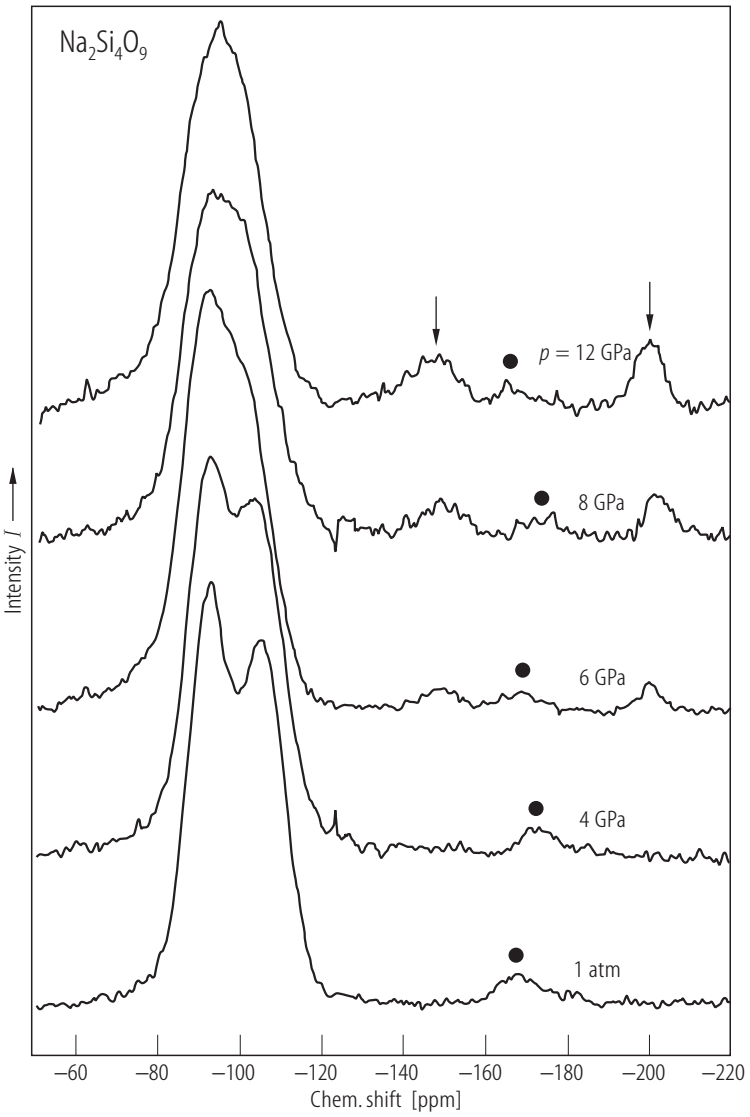

Fig. 18. $Na_2Si_4O_9$. Glasses. ^{29}Si MAS NMR spectra of samples quenched from liquid at 1 atm and 1200 °C, 4 GPa and 1800 °C, 6 GPa and 1900 °C, 8 GPa and 2000 °C and 12 GPa and 2100 °C [91X1]. Solid dots show spinning side bands and arrows show positions of the peaks due to $^{[5]}Si$ and $^{[6]}Si$.

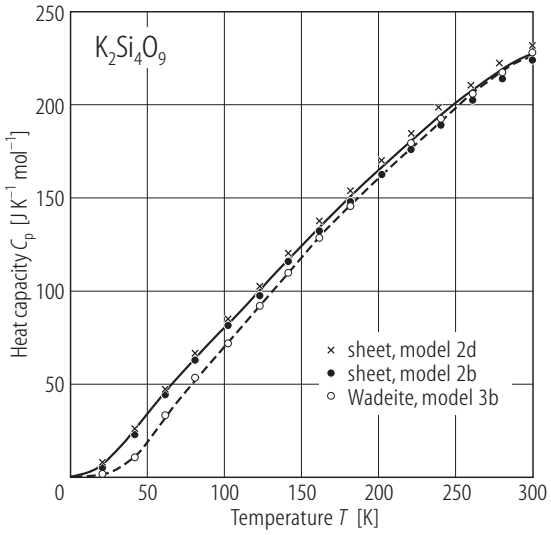

Fig. 19. $K_2Si_4O_9$. Calculated low-temperature heat capacities of low- and high-pressure forms [87G1].

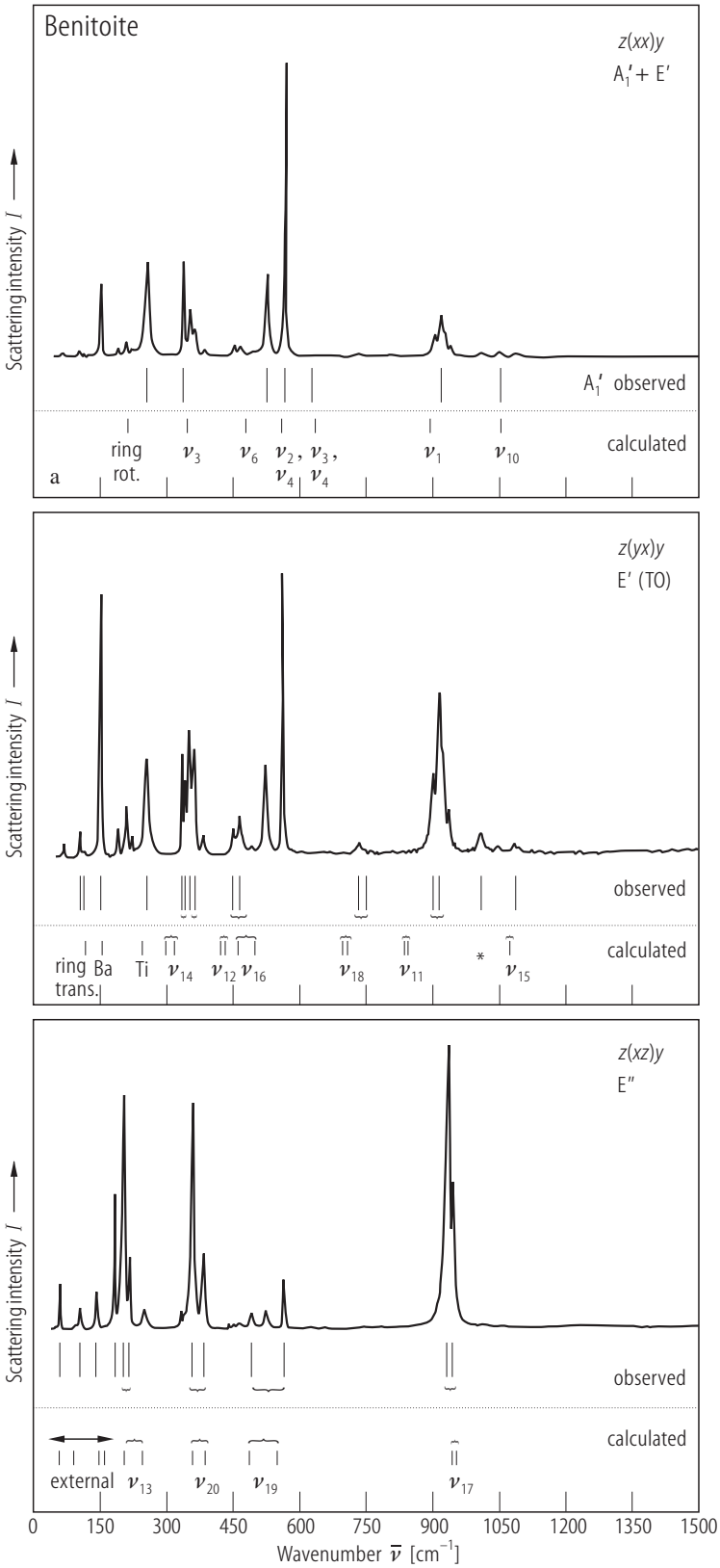

Fig. 20. Benitoite, $BaTiSi_3O_9$. Raman spectra. **(a)** The A'_1+ E′ spectrum with the A'_1 species lines indicated; intensity maximum is 10^5 counts; **(b)** the E' spectrum; intensity maximum is $2 \cdot 10^4$ counts. Mixtures of calculated internal ring modes occur from 300…800 cm^{-1}. Most prominent eigenmode for a particular calculated frequency is listed. The asterisked line at 993 cm^{-1} is probably a combination mode; **(c)** the E" spectrum; intensity maximum is $6 \cdot 10^4$ counts. The group of calculated frequencies labeled as external have eigenmodes which are mixtures of Ba translation, Ti translation, ring rotation and υ_{13}. Most prominent eigenmode for a particular calculated frequency is indicated. For all figures the observed frequencies are plotted above those calculated for that species [93M1].

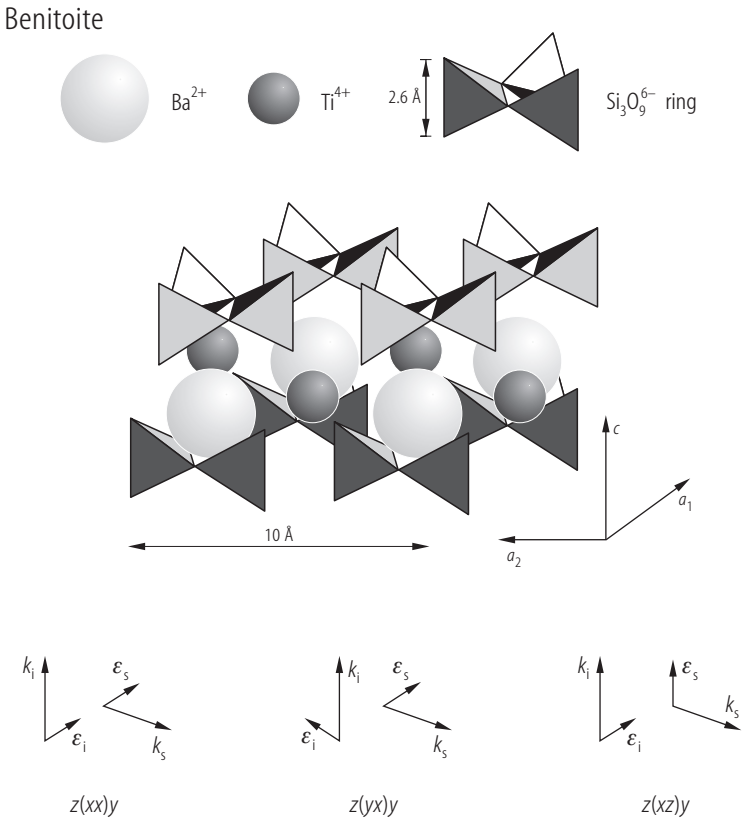

Fig. 21. Benitoite. Orientation of the crystal structure with respect to incident and scattered light for the A'_1+ E′, E' and E" spectra. The incident light propagation direction is $\boldsymbol{k}_i$ and its polarization direction is $\boldsymbol{\varepsilon}_i$. The scattered light propagation is $\boldsymbol{k}_s$ and its polarization direction is $\boldsymbol{\varepsilon}_s$ [93M1].

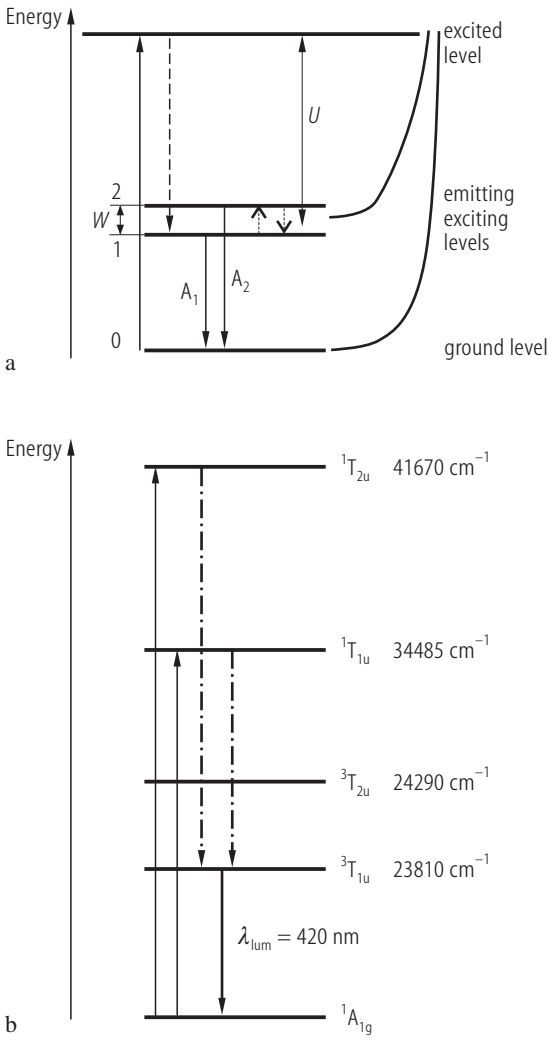

Fig. 22. Benitoite. (**a)** Calculated energy levels scheme for blue luminescence. **(b)** Energy level scheme for the TiO_6 luminescence center [04G1].

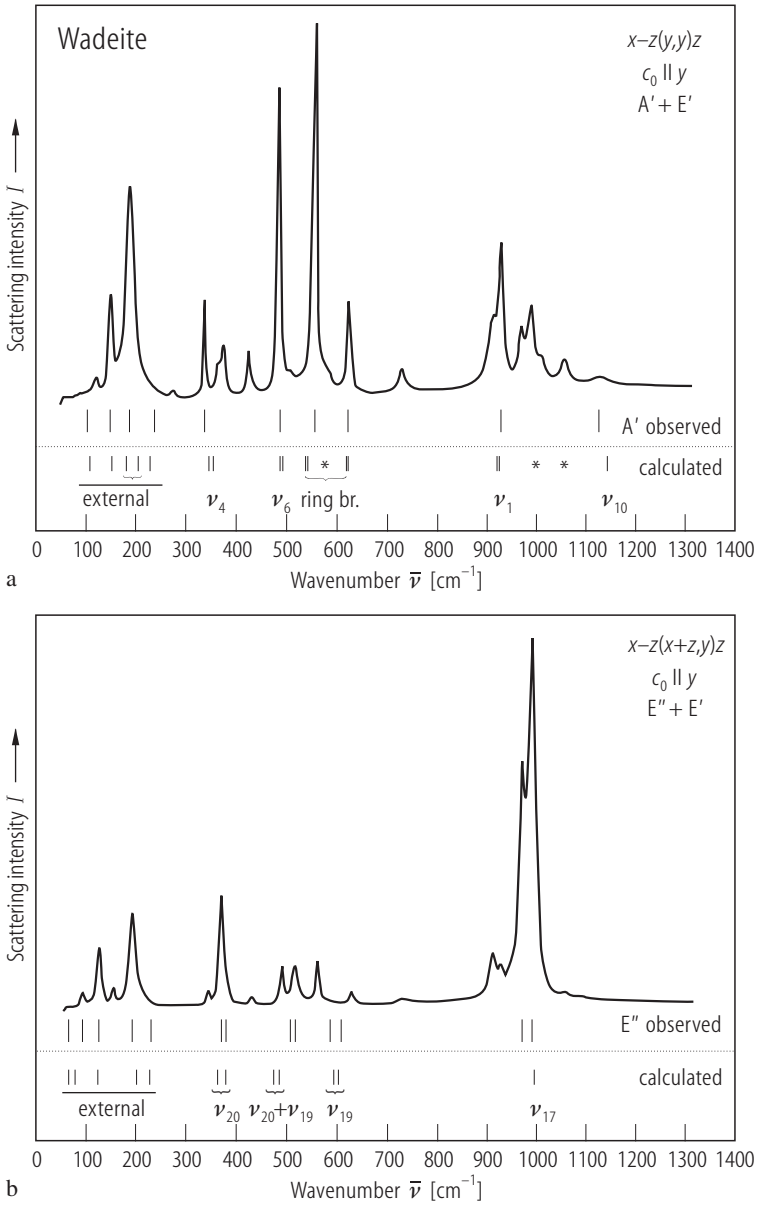

Fig. 23. Wadeite (natural). Measured Raman spectra. **(a)** A'+E' symmetries. Below, fundamental A' frequencies are indicated as vertical bars. Labeled as calculated are the theoretical A' frequencies plotted as vertical bars and some vibrational assignments from the normal coordinate analysis. Labeled as (*) are combination or overtone modes and as "ring br." are ring breathing modes. **(b)** E"+E' symmetries with the E" modes being dominant. Fundamental E" frequencies are indicated as vertical bars [96M1].

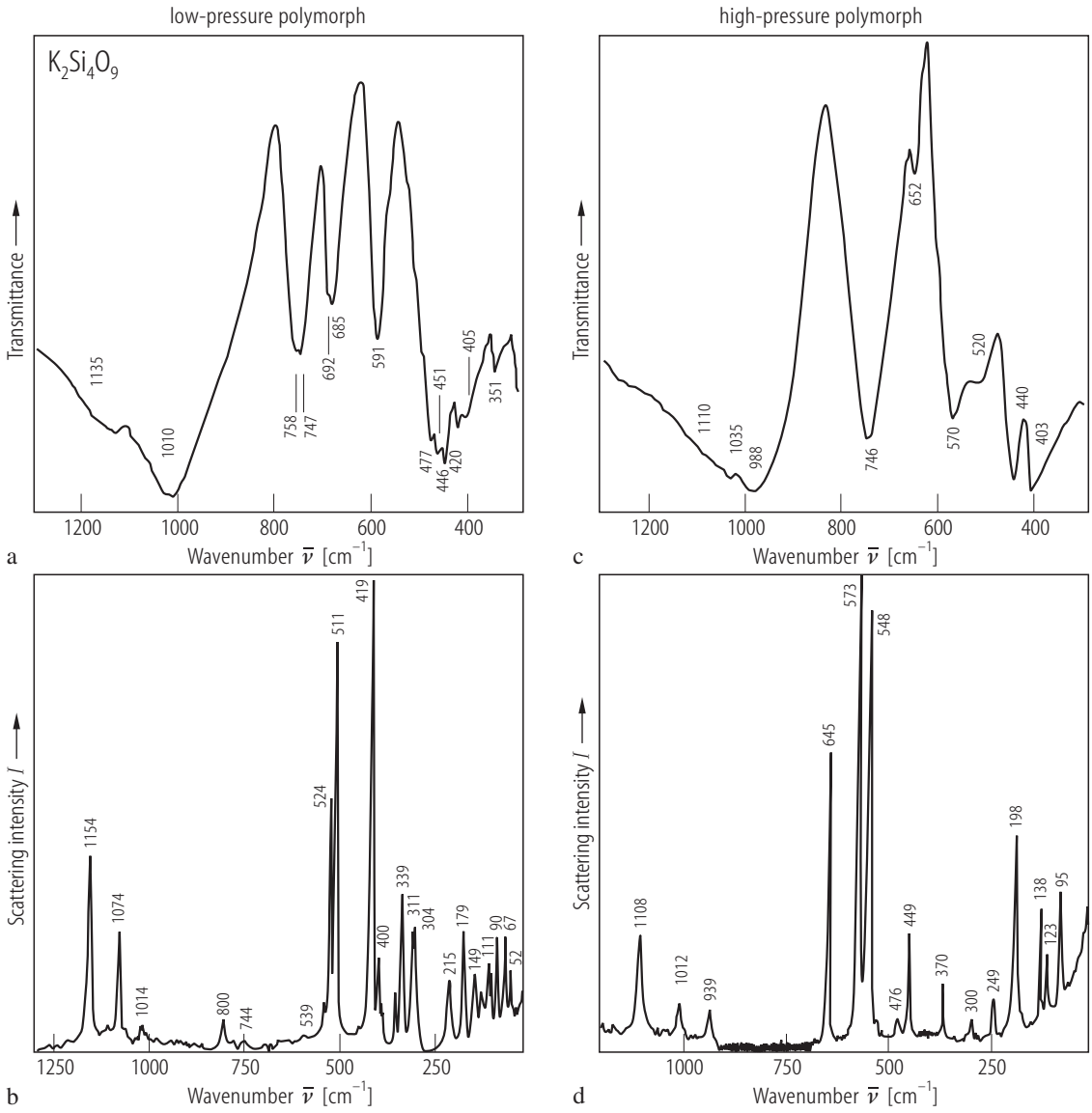

Fig. 24. $K_2Si_4O_9$. Low-pressure form, **(a)** infrared spectrum, **(b)** Raman spectrum. High-pressure form (wadeite type), **(c)** infrared spectrum, **(d)** Raman spectrum [87G1].

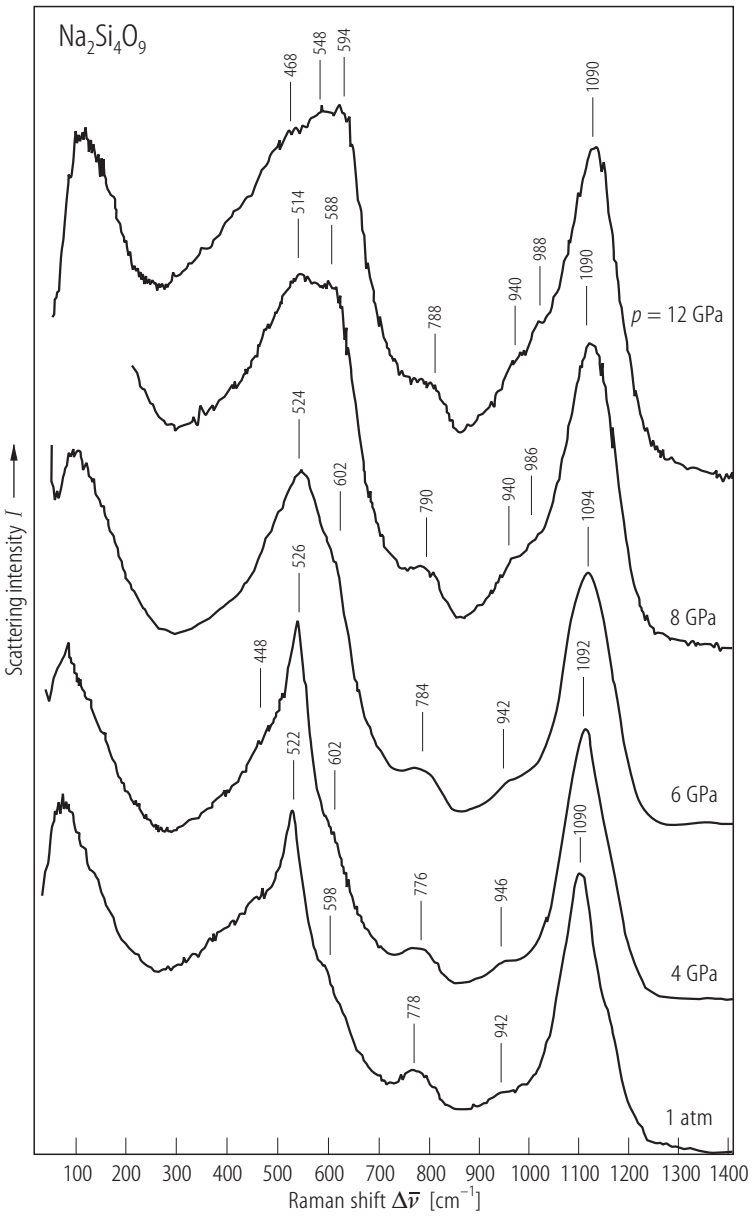

Fig. 25. $Na_2Si_4O_9$. Glasses. Unpolarized Raman spectra of samples with 95 % ^{29}Si enriched compositions [91X1].

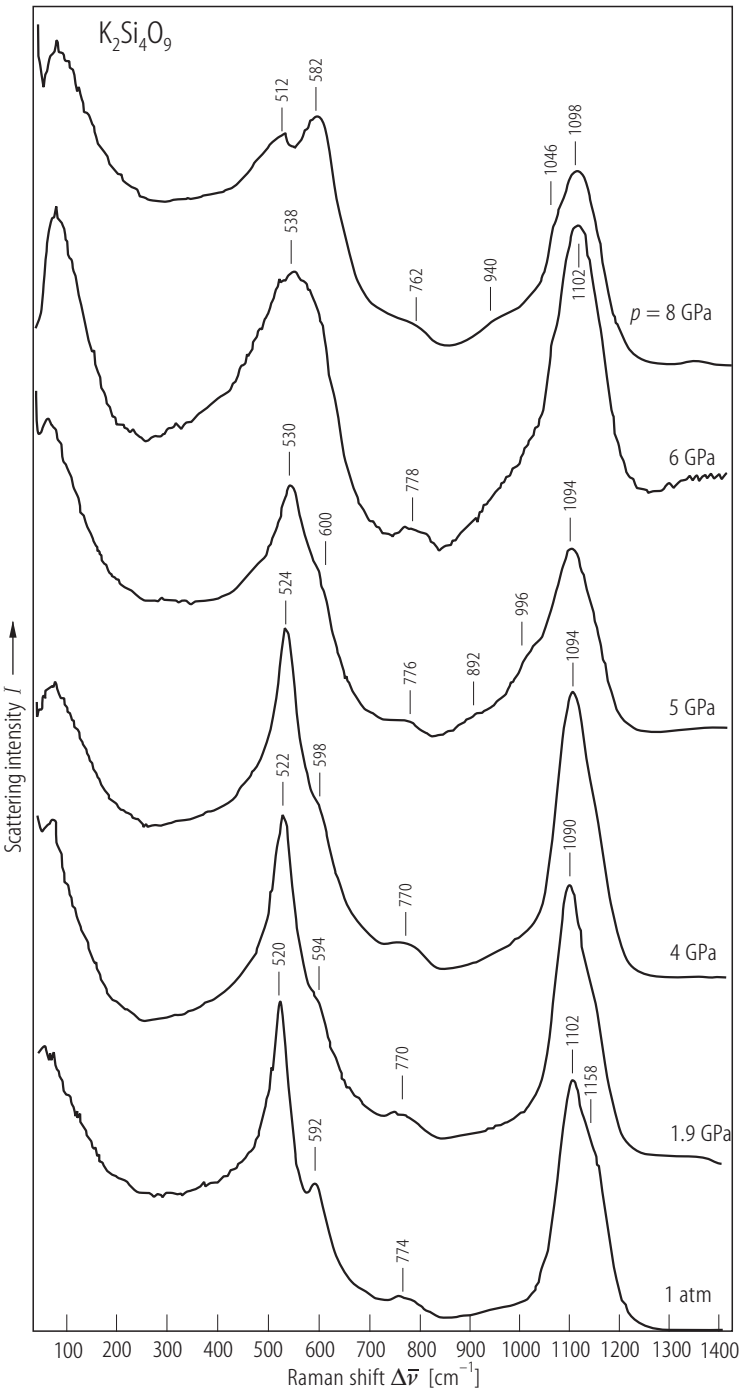

Fig. 26. $K_2Si_4O_9$. Glasses. Unpolarized Raman spectra of samples quenched from liquids at various pressures [91X1]. The samples quenched at 1 atm and 5, 6 and 9 GPa have normal Si isotopic abundance.

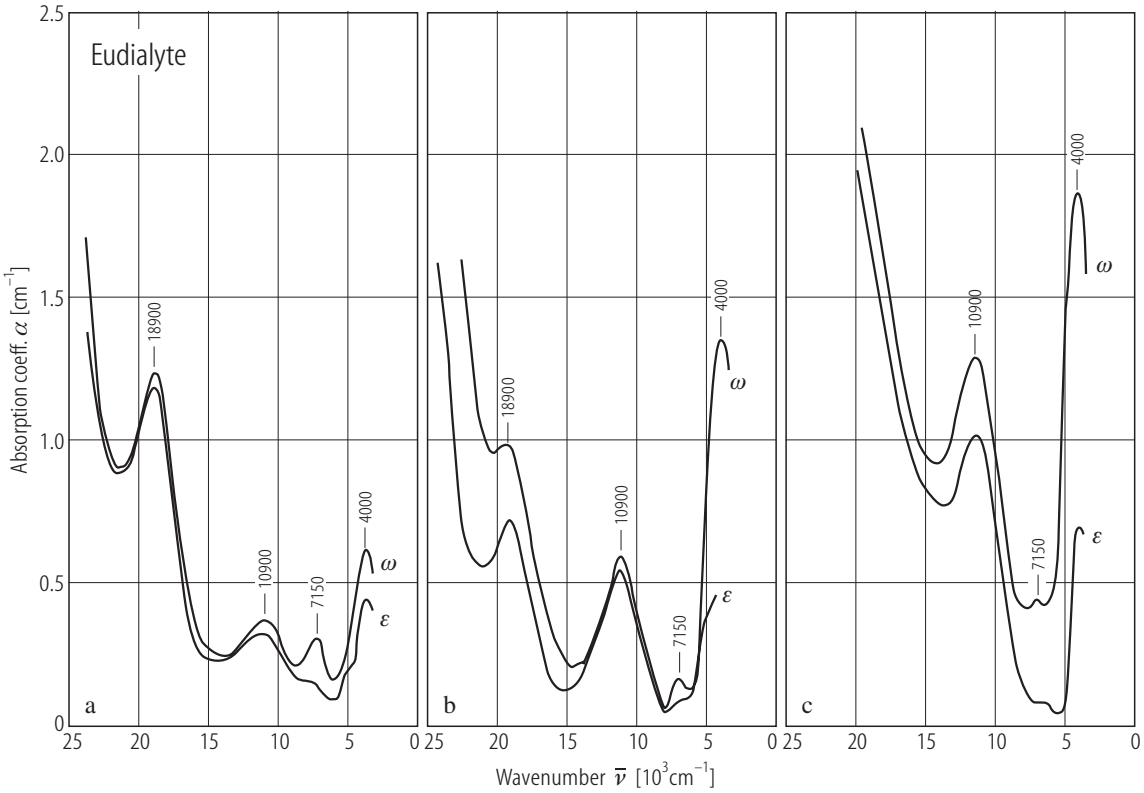

Fig. 27. Eudialyte. Optical absorption spectra: **(a)** crimson[12)] and pink, optically positive; **(b)** red-brown[15)] intermediate variety; **(c)** brown and yellow-brown[14)], optically negative [91P1].

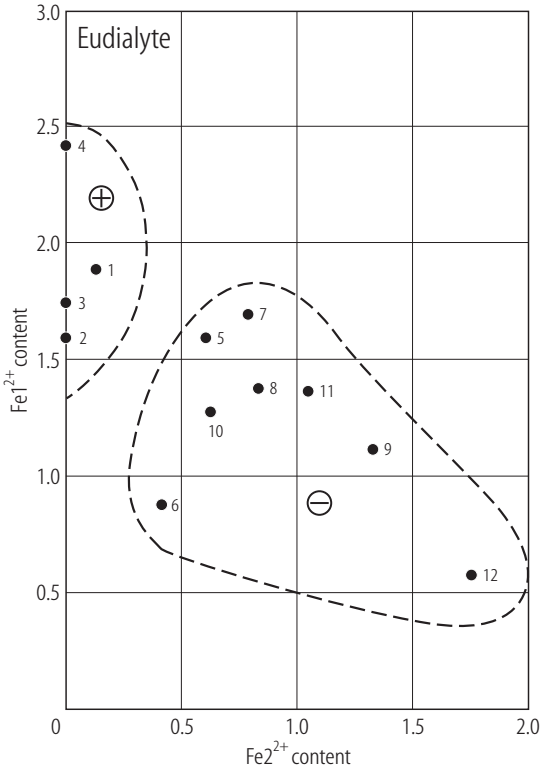

Fig. 28. Eudialyte. Relative content of $Fe1^{2+}$ and $Fe2^{2+}$. Dashed lines denote fields of optically positive and optically negative varieties [91P1].